Theory of the lattice Boltzmann equation: Lattice Boltzmann model for axisymmetric flows

Zhaoli Guo,* Haifeng Han, Baochang Shi,† and Chuguang Zheng
National Laboratory of Coal Combustion, Huazhong University of Science and Technology, Wuhan 430074, China
(Received 16 December 2008; published 20 April 2009)

A lattice Boltzmann equation (LBE) for axisymmetric flows is proposed. The model has some distinct features that distinguish it from existing axisymmetric LBE models. First, it is derived from the Boltzmann equation so that it has a solid physics base and is easy for generalization; second, the model can describe the axial, radial, and azimuthal velocity components in the same fashion; and third, the source terms of the model contain no velocity gradients and are much simpler than other LBE models. Numerical tests, including steady and unsteady internal and external flows, demonstrate that the proposed LBE can serve as a viable and efficient method for low speed axisymmetric flows.

DOI: 10.1103/PhysRevE.79.046708 PACS number(s): 47.11.−j, 02.60.Cb, 47.45.Ab

I. INTRODUCTION

Axisymmetric flows of incompressible fluids are frequently encountered in fundamental researches in fluid dynamics. Such flows can be treated as a two-dimensional (2D) problem in the meridian plane so that computational costs can be significantly reduced compared with fully three-dimensional (3D) computations. The lattice Boltzmann equation (LBE), which appeared as an effective mesoscopical method for modeling and simulating fluid flows about two decades ago [1–5], has also been applied to axisymmetric flows recently. The most natural way for LBE to simulate an axisymmetric flow is the direct application of certain 3D LBE models with suitable curved boundary conditions [6–8]. However, such approaches do not take any advantages of the axisymmetric properties of the flow and usually need large computational costs.

Alternatively, some researchers have attempted to develop more effective quasi-2D LBE models for solving the hydrodynamic equations in axisymmetric formulations. The first axisymmetric LBE model was attributed to Halliday *et al.* [9], who introduced some source terms into the LBE so that it could match the axisymmetric Navier-Stokes equations in the Chapman-Enskog analysis. The method was also extended to multiphase flows by considering intermolecular interactions among fluids [10,11]. Unfortunately, the method by Halliday *et al.* [9] fails to reproduce the correct hydrodynamic momentum equation due to some missing terms relating to the radial velocity. This mismatch was pointed out by Lee *et al.* [12]. After considering these missing terms, Lee *et al.* [12] were able to develop a more accurate axisymmetric LBE model. Reis and Phillips [13,14] proposed a similar model soon after. Zhou [15] recently proposed another simplified version where the forcing terms are similar to those in the hydrodynamic equations. The above LBE models are constructed based on the Navier-Stokes equations with primitive variables, while Chen *et al.* [16] recently showed that it was also possible to obtain a LBE model for the vorticity-stream equations.

Compared with the full 3D models, the main advantage of the 2D axisymmetric LBE models mentioned above lies in their high efficiency in computations. Actually, these models have been successfully applied to various flows, ranging from continuous single phase flows to microscale and two phase flows [17–25]. However, these models still have some limitations. First of all, all of the available models are designed in a "top-down" fashion, i.e., they are all constructed based on the axisymmetric hydrodynamic equations, and actually have no relevance to the kinetic theory (Boltzmann equation). In this regard, these LBE models are nothing but numerical solvers for the axisymmetric Navier-Stokes equations. Consequently, some of important advantages of LBE, such as the easy in describing microscopical interactions in multicomponent/multiphase systems, applicability for complex fluid systems without suitable governing equations, and flows that cannot be described by continuum models, may be lost. Second, in all of the existing axisymmetric LBE models the azimuthal velocity is neglected although some hybrid methods, where the equation for the azimuthal velocity is solved by finite-difference method, were used in some applications [17,18,21]. Such models are suitable for axisymmetric flows with a negligible azimuthal component of velocity. But in general cases, particularly for rotating and/or swirling flows, the azimuthal velocity must be considered. From this viewpoint, these LBE models are *incomplete* and their applicability is limited. Finally, almost all of the available models (except for the one in [16]) contain some complicated source terms including many velocity gradients. The discretization of these terms not only makes the implementations rather cumbersome but also may introduce additional errors and lead to numerical instability. The source terms in the method by Zhou [15] are simple relatively, but they still contain velocity gradients and are implicit in the evolution equation; on the other hand, the method in [16] simplified the source terms by invoking the vorticity-stream formulation, but it will become very inefficient for unsteady flows because a Poisson equation must be solved at every time step.

In this paper, we aim to develop a simple and consistent axisymmetric LBE based on the continuous Boltzmann equation. The model can describe the velocities in all directions and therefore is *complete*. The rest of the paper is organized as follows. In Sec. II a simple kinetic model is proposed for axisymmetric flows, and in Sec. III a LBE model is devel-

*zlguo@mail.hust.edu.cn
†sbchust@yahoo.com

oped based on the kinetic model. Boundary conditions and force evaluation methods are discussed in Sec. IV, and some numerical simulations are carried out in Sec. V to test the performance of the LBE model. Finally a brief summary is presented in Sec. VI.

II. SIMPLIFIED AXISYMMETRIC BHATNAGAR-GROSS-KROOK MODEL

In a system of cylindrical coordinates (x,r,θ), where x, r, and θ are the axial, radial, and azimuthal coordinates, respectively, the Boltzmann equation with the Bhatnagar-Gross-Krook (BGK) collision model reads

$$\frac{\partial f}{\partial t}+\xi_x\frac{\partial f}{\partial x}+\xi_r\frac{\partial f}{\partial r}+\frac{\xi_\theta}{r}\frac{\partial f}{\partial \theta}+\frac{\xi_\theta^2}{r}\frac{\partial f}{\partial \xi_r}-\frac{\xi_r\xi_\theta}{r}\frac{\partial f}{\partial \xi_\theta}=-\frac{1}{\tau}[f-f^{(\mathrm{eq})}], \tag{1}$$

where $f(\boldsymbol{x}_0,\boldsymbol{\xi}_0,t)\equiv f(x,r,\theta,\xi_x,\xi_r,\xi_\theta,t)$ is the distribution function of fluid molecules moving with velocity $\boldsymbol{\xi}_0=(\xi_x,\xi_r,\xi_\theta)$ at position $\boldsymbol{x}_0=(x,r,\theta)$ and time t in the cylindrical coordinates; τ is the relaxation time characterizing the relaxation process from f toward the local Maxwellian equilibrium distribution $f^{(\mathrm{eq})}$ defined by

$$f^{(\mathrm{eq})}=\frac{\rho}{(2\pi RT)^{3/2}}\exp\left[-\frac{|\boldsymbol{\xi}_0-\boldsymbol{u}_0|^2}{2RT}\right],$$

where R is the gas constant and ρ, $\boldsymbol{u}_0=(u_x,u_r,u_\theta)$, and T are the fluid density, velocity, and temperature defined, respectively, by

$$\rho=\int f d\boldsymbol{\xi}_0,\quad \rho\boldsymbol{u}_0=\int \boldsymbol{\xi} f d\boldsymbol{\xi}_0,\quad 3\rho RT=\int |\boldsymbol{\xi}_0-\boldsymbol{u}_0|^2 f d\boldsymbol{\xi}_0. \tag{2}$$

For symmetric flows f does not depend on the θ-coordinate and the flow becomes quasi-two-dimensional [26]. In order to reduce the number of independent variables, we introduce two reduced distribution functions,

$$\tilde{f}(\boldsymbol{x},\boldsymbol{\xi})=\int f d\xi_\theta,\quad \bar{f}(\boldsymbol{x},\boldsymbol{\xi})=\int \xi_\theta f d\xi_\theta, \tag{3}$$

where $\boldsymbol{x}=(x,r)$ and $\boldsymbol{\xi}=(\xi_x,\xi_r)$ are the corresponding position and molecular velocity in a meridian plane. From Eq. (1), we can obtain two model equations for $\tilde{f}$ and $\bar{f}$,

$$\frac{\partial \tilde{f}}{\partial t}+\boldsymbol{\xi}\cdot\boldsymbol{\nabla}\tilde{f}+\frac{\xi_r}{r}\tilde{f}+\frac{1}{r}\frac{\partial \tilde{\phi}}{\partial \xi_r}=-\frac{1}{\tau}[\tilde{f}-\tilde{f}^{(\mathrm{eq})}], \tag{4}$$

$$\frac{\partial \bar{f}}{\partial t}+\boldsymbol{\xi}\cdot\boldsymbol{\nabla}\bar{f}+\frac{2\xi_r}{r}\bar{f}+\frac{1}{r}\frac{\partial \bar{\phi}}{\partial \xi_r}=-\frac{1}{\tau}[\bar{f}-\bar{f}^{(\mathrm{eq})}], \tag{5}$$

where $\boldsymbol{\nabla}=(\partial_x,\partial_r)$ is the spatial gradient operator in terms of $\mathbf{x}$, and

$$\tilde{\phi}(\boldsymbol{x},\boldsymbol{\xi})=\int \xi_\theta^2 f d\xi_\theta,\quad \bar{\phi}(\boldsymbol{x},\boldsymbol{\xi})=\int \xi_\theta^3 f d\xi_\theta.$$

The corresponding reduced equilibrium distribution functions are given, respectively, by

$$\tilde{f}^{(\mathrm{eq})}=\frac{\rho}{2\pi RT}\exp\left[-\frac{|\boldsymbol{\xi}-\boldsymbol{u}|^2}{2RT}\right],\quad \bar{f}^{(\mathrm{eq})}=u_\theta\tilde{f}^{(\mathrm{eq})},$$

where $\boldsymbol{u}=(u_x,u_r)$ is the corresponding velocity in the meridian plane. From Eq. (2), the fluid variables can be readily computed from the reduced distribution functions as

$$\rho=\int \tilde{f}d\boldsymbol{\xi},\quad \rho\boldsymbol{u}=\int \boldsymbol{\xi}\tilde{f}d\boldsymbol{\xi},\quad \rho u_\theta=\int \bar{f}d\boldsymbol{\xi},$$

$$3\rho RT+\rho|\boldsymbol{u}_0|^2=\int |\boldsymbol{\xi}|^2\tilde{f}d\boldsymbol{\xi}+\int \tilde{\phi}d\boldsymbol{\xi}. \tag{6}$$

The last two terms relevant to $\tilde{\phi}$ and $\bar{\phi}$ on the left-hand sides of Eqs. (4) and (5) cannot be expressed explicitly. Now we propose some approximations to them without affecting the corresponding hydrodynamic equations. To this end, we first perform a Chapman-Enskog analysis for both equations to find out necessary constraints for such approximations. For simplicity, we consider isothermal flows only ($RT=$const).

In the Chapman-Enskog analysis, we introduce the following expansions,

$$\partial_t=\sum_{n=0}^{\infty}\tau^n\partial_{t_n},\quad f=\sum_{n=0}^{\infty}\tau^n f^{(n)}. \tag{7}$$

The expansion of f leads to

$$\tilde{f}=\sum_{n=0}^{\infty}\tau^n\tilde{f}^{(n)},\quad \bar{f}=\sum_{n=0}^{\infty}\tau^n\bar{f}^{(n)}. \tag{8}$$

Substituting these expansions into Eqs. (1), (4), and (5), we can obtain the following set of successive equations in the order of τ:

$$\tau^0:\quad f^{(0)}=f^{(\mathrm{eq})},\quad \tilde{f}^{(0)}=\tilde{f}^{(\mathrm{eq})},\quad \bar{f}^{(0)}=\bar{f}^{(\mathrm{eq})}, \tag{9}$$

$$\tau^1:\quad D_{t_0}f^{(0)}+\frac{\xi_\theta^2}{r}\frac{\partial f^{(0)}}{\partial \xi_r}-\frac{\xi_r\xi_\theta}{r}\frac{\partial f^{(0)}}{\partial \xi_\theta}=-f^{(1)}, \tag{10}$$

$$D_{t_0}\tilde{f}^{(0)}+\frac{\xi_r}{r}\tilde{f}^{(0)}+\frac{1}{r}\frac{\partial \tilde{\phi}^{(0)}}{\partial \xi_r}=-\tilde{f}^{(1)}, \tag{11}$$

$$D_{t_0}\bar{f}^{(0)}+\frac{2\xi_r}{r}\bar{f}^{(0)}+\frac{1}{r}\frac{\partial \bar{\phi}^{(0)}}{\partial \xi_r}=-\bar{f}^{(1)}, \tag{12}$$

$$\tau^2:\quad \frac{\partial \tilde{f}^{(0)}}{\partial t_1}+D_{t_0}\tilde{f}^{(1)}+\frac{\xi_r}{r}\tilde{f}^{(1)}+\frac{1}{r}\frac{\partial \tilde{\phi}^{(1)}}{\partial \xi_r}=-\tilde{f}^{(2)}, \tag{13}$$

$$\frac{\partial \bar{f}^{(0)}}{\partial t_1}+D_{t_0}\bar{f}^{(1)}+\frac{2\xi_r}{r}\bar{f}^{(1)}+\frac{1}{r}\frac{\partial \bar{\phi}^{(1)}}{\partial \xi_r}=-\bar{f}^{(2)}, \tag{14}$$

where $D_{t_0}=\partial_{t_0}+\boldsymbol{\xi}\cdot\boldsymbol{\nabla}$ and $\tilde{\phi}^{(n)}$ and $\bar{\phi}^{(n)}$ are the corresponding expansion terms of $\tilde{\phi}$ and $\bar{\phi}$, respectively,

$$\tilde{\phi}^{(n)} = \int \xi_\theta^2 f^{(n)} d\xi_\theta, \quad \bar{\phi}^{(n)} = \int \xi_\theta^3 f^{(n)} d\xi_\theta.$$

Particularly,

$$\tilde{\phi}^{(0)} = (u_\theta^2 + RT)\tilde{f}^{(0)}, \quad \bar{\phi}^{(0)} = (u_\theta^2 + 3RT)\bar{f}^{(0)}. \tag{15}$$

It is also obvious that

$$\int \frac{\partial \tilde{\phi}^{(n)}}{\partial \xi_r} d\boldsymbol{\xi} = \int \frac{\partial \bar{\phi}^{(n)}}{\partial \xi_r} d\boldsymbol{\xi} = 0,$$

$$\int \xi_\alpha \frac{\partial \tilde{\phi}^{(n)}}{\partial \xi_r} d\boldsymbol{\xi} = -\delta_{\alpha r} \int \tilde{\phi}^{(n)} d\boldsymbol{\xi}. \tag{16}$$

Therefore, based on the definitions of the fluid variables and the original and reduced equilibrium distribution functions, we can obtain that

$$\int \tilde{f}^{(n)} d\boldsymbol{\xi} = \int \bar{f}^{(n)} d\boldsymbol{\xi} = 0, \quad \int \boldsymbol{\xi} \tilde{f}^{(n)} d\boldsymbol{\xi} = 0 \tag{17}$$

for $n > 0$. With the aids of Eqs. (16) and (17), the first-order hydrodynamic equations can be obtained by taking zeroth and first velocity moments of Eqs. (11) and (12),

$$\partial_{t_0} \rho + \boldsymbol{\nabla} \cdot (\rho \boldsymbol{u}) + \frac{\rho u_r}{r} = 0, \tag{18a}$$

$$\partial_{t_0}(\rho u_\alpha) + \partial_\beta(\rho u_\alpha u_\beta + p\delta_{\alpha\beta}) = \frac{\rho u_\theta^2}{r}\delta_{\alpha r} - \frac{\rho u_\alpha u_r}{r}, \tag{18b}$$

$$\partial_{t_0}(\rho u_\theta) + \partial_\beta(\rho u_\beta u_\theta) = -\frac{2\rho u_\theta u_r}{r}, \tag{18c}$$

where $p = \rho RT$ is the pressure. Note that in the derivation of Eqs. (18b) and (18c) we have made use of Eq. (15).

Similarly, by taking velocity moments of Eqs. (13) and (14) we can obtain the following equations at $O(\tau^2)$:

$$\partial_{t_1} \rho = 0, \tag{19a}$$

$$\partial_{t_1}(\rho u_\alpha) + \partial_\beta P_{\alpha\beta}^{(1)} + \frac{1}{r} P_{\alpha r}^{(1)} - \frac{\delta_{\alpha r}}{r} \int \bar{\phi}^{(1)} d\boldsymbol{\xi} = 0, \tag{19b}$$

$$\partial_{t_1}(\rho u_\theta) + \partial_\beta Q_\beta^{(1)} + \frac{2}{r} Q_r^{(1)} = 0, \tag{19c}$$

where

$$P_{\alpha\beta}^{(1)} = \int \xi_\alpha \xi_\beta \tilde{f}^{(1)} d\boldsymbol{\xi}, \quad Q_\beta^{(1)} = \int \xi_\beta \bar{f}^{(1)} d\boldsymbol{\xi}.$$

These two integrals can be evaluated by making use of Eqs. (11) and (12) and the first-order hydrodynamic equations [Eq. (18)]. After some tedious but standard algebra we get that

$$P_{\alpha\beta}^{(1)} = -p(\partial_\alpha u_\beta + \partial_\beta u_\alpha), \quad Q_\beta^{(1)} = \frac{p u_\theta}{r}\delta_{\beta r} - p\partial_\beta u_\theta, \tag{20}$$

where terms of $O(M_a^2)$ have been neglected (M_a is the Mach number of the flow).

Now we evaluate the last term on the left-hand side of Eq. (19b). First, from Eqs. (10) and (18) we can obtain that

$$\begin{aligned} -\int \bar{\phi}^{(1)} d\boldsymbol{\xi} &= -\int \xi_\theta^2 f^{(1)} d\boldsymbol{\xi} d\xi_\theta \\ &= \partial_{t_0} \int \tilde{\phi}^{(0)} d\boldsymbol{\xi} + \partial_\beta \int \xi_\beta \tilde{\phi}^{(0)} d\boldsymbol{\xi} + \frac{3}{r} \int \xi_r \tilde{\phi}^{(0)} d\boldsymbol{\xi} \\ &= \partial_{t_0}(\rho u_\theta^2 + \rho RT) + \partial_\beta[\rho u_\beta (u_\theta^2 + RT)] \\ &\quad + \frac{3\rho u_r}{r}(u_\theta^2 + RT) \\ &= RT\left[\partial_{t_0}\rho + \partial_\beta(\rho u_\beta) + \frac{\rho u_r}{r}\right] + \partial_{t_0}(\rho u_\theta^2) \\ &\quad + \partial_\beta(\rho u_\beta u_\theta^2) + \frac{\rho u_r}{r}(2RT + 3u_\theta^2) \\ &= \frac{2p u_r}{r}. \end{aligned} \tag{21}$$

Therefore, combining the first- and second-order equations [Eqs. (18) and (19)], we can obtain the final axisymmetric hydrodynamic equations,

$$\partial_t \rho + \partial_\alpha(\rho u_\alpha) + \frac{\rho u_r}{r} = 0, \tag{22a}$$

$$\begin{aligned} &\partial_t(\rho u_\alpha) + \partial_\beta(\rho u_\alpha u_\beta) \\ &= -\partial_\alpha p + \partial_\beta[\mu(\partial_\alpha u_\beta + \partial_\beta u_\alpha)] + \frac{\mu}{r}(\partial_r u_\alpha + \partial_\alpha u_r) \\ &\quad + \frac{\rho u_\theta^2}{r}\delta_{\alpha r} - \frac{\rho u_\alpha u_r}{r} - \frac{2\mu}{r^2} u_r \delta_{\alpha r}, \end{aligned} \tag{22b}$$

$$\begin{aligned} &\partial_t(\rho u_\theta) + \partial_\beta(\rho u_\beta u_\theta) \\ &= \partial_\beta(\mu \partial_\beta u_\theta) - \frac{2\rho u_\theta u_r}{r} - \frac{\mu}{r}\left(u_\theta \partial_r \ln \rho - \partial_r u_\theta + \frac{u_\theta}{r}\right), \end{aligned} \tag{22c}$$

where $\mu = \tau p$ is the dynamic viscosity. In the incompressible limit with $\rho \approx$ const, the above equations can be rearranged as

$$\frac{\partial u_x}{\partial x} + \frac{1}{r}\frac{\partial (r u_r)}{\partial r} = 0, \tag{23a}$$

$$\rho \frac{du_x}{dt} = -\frac{\partial p}{\partial x} + \mu\left[\frac{1}{r}\frac{\partial}{\partial r}\left(r\frac{\partial u_x}{\partial r}\right) + \frac{\partial^2 u_x}{\partial x^2}\right], \tag{23b}$$

$$\rho \frac{du_r}{dt} = -\frac{\partial p}{\partial r} + \mu\left[\frac{\partial}{\partial r}\left(\frac{1}{r}\frac{\partial (r u_r)}{\partial r}\right) + \frac{\partial^2 u_r}{\partial x^2}\right] + \frac{u_\theta^2}{r}, \tag{23c}$$

$$\rho\frac{du_\theta}{dt}=\mu\left[\frac{\partial}{\partial r}\left(\frac{1}{r}\frac{\partial(ru_\theta)}{\partial r}\right)+\frac{\partial^2 u_\theta}{\partial x^2}\right], \tag{23d}$$

where

$$\frac{d\phi}{dt}=\frac{\partial\phi}{\partial t}+\frac{\partial(u_x\phi)}{\partial x}+\frac{1}{r}\frac{\partial(ru_r\phi)}{\partial r}$$

for any variable ϕ. Equations (23) are just the incompressible Navier-Stokes equations for axisymmetric flows [27].

We can see that in the above analysis the exact expressions of $\tilde{\phi}^{(1)}$ and $\bar{\phi}^{(1)}$ are not required. However, they must satisfy some necessary properties, i.e., Eqs. (16) and (21), which are critical for obtaining the final hydrodynamic equations. This fact indicates that if we can approximate them with some simple formulations satisfying both properties, the final hydrodynamic equations will not change. One such choice is

$$\tilde{\phi}^{(1)}=-\frac{2RTu_r}{r}\tilde{f}^{(\mathrm{eq})},\quad \bar{\phi}^{(1)}=0,\quad \tilde{\phi}^{(k)}=\bar{\phi}^{(k)}=0\quad (k>1). \tag{24}$$

As such, $\tilde{\phi}$ and $\bar{\phi}$ can be written explicitly as

$$\tilde{\phi}=\tilde{\phi}^{(0)}+\tau\tilde{\phi}^{(1)}=\left(u_\theta^2+RT-\frac{2\tau RTu_r}{r}\right)\tilde{f}^{(\mathrm{eq})},$$

$$\bar{\phi}=\bar{\phi}^{(0)}=(u_\theta^2+3RT)\bar{f}^{(\mathrm{eq})}. \tag{25}$$

With these expressions we obtain the following BGK model for axisymmetric flow from Eqs. (4) and (5):

$$\frac{\partial\tilde{f}}{\partial t}+\boldsymbol{\xi}\cdot\boldsymbol{\nabla}\tilde{f}+\frac{\xi_r}{r}\tilde{f}+\tilde{\Phi}=-\frac{1}{\tau}[\tilde{f}-\tilde{f}^{(\mathrm{eq})}], \tag{26}$$

$$\frac{\partial\bar{f}}{\partial t}+\boldsymbol{\xi}\cdot\boldsymbol{\nabla}\bar{f}+\frac{2\xi_r}{r}\bar{f}+\bar{\Phi}=-\frac{1}{\tau}[\bar{f}-\bar{f}^{(\mathrm{eq})}], \tag{27}$$

where

$$\tilde{\Phi}=\frac{1}{r}\frac{\partial\tilde{\phi}}{\partial\xi_r}=-\left(1+\frac{u_\theta^2}{RT}-\frac{2\tau u_r}{r}\right)\frac{\xi_r-u_r}{r}\tilde{f}^{(\mathrm{eq})}, \tag{28}$$

$$\bar{\Phi}=\frac{1}{r}\frac{\partial\bar{\phi}}{\partial\xi_r}=-\left(3+\frac{u_\theta^2}{RT}\right)\frac{\xi_r-u_r}{r}\bar{f}^{(\mathrm{eq})}. \tag{29}$$

It should be emphasized that other approximations to $\tilde{\phi}$ and $\bar{\phi}$ are also possible. For instance, another choice for $\tilde{\phi}^{(1)}$ that satisfies Eq. (21) is $\tilde{\phi}^{(1)}=-(2RT\xi_r/r)\tilde{f}^{(\mathrm{eq})}$. With such an approximation, $\tilde{\Phi}$ can be expressed as

$$\tilde{\Phi}=-\left(1+\frac{u_\theta^2}{RT}-\frac{2\tau\xi_r}{r}\right)\frac{\xi_r-u_r}{r}\tilde{f}^{(\mathrm{eq})}-\frac{2RT}{r}\tilde{f}^{(\mathrm{eq})}, \tag{30}$$

which is a little more complicated than that given by Eq. (28). Furthermore, as can be seen later, $\tilde{\Phi}$ given by Eq. (28) can be combined with the forcing term due to external forces, and the final LBE model has a simple structure. On the other hand, the approximation given by Eq. (30) cannot be combined with the forcing term so easily and would make the final LBE more complicated. From this viewpoint, the approximation given by Eq. (24) may be one of the simplest formulations (if not the only one).

In the above discussions the external force is not considered. If the fluid is also exposed to a force field $\boldsymbol{F}=\rho\boldsymbol{a}_0\equiv\rho(a_x,a_r,a_\theta)$, the Boltzmann equation [Eq. (1)] should be modified to include a forcing term F on the left-hand side, where F is defined by

$$F\equiv\boldsymbol{a}_0\cdot\boldsymbol{\nabla}_{\boldsymbol{\xi}_0}f=a_x\frac{\partial f}{\partial\xi_x}+a_r\frac{\partial f}{\partial\xi_r}+a_\theta\frac{\partial f}{\partial\xi_\theta}.$$

Here we assume that the force does not depend on the molecular velocity $\boldsymbol{\xi}_0$. As suggested in [28], the forcing term can be approximated as

$$F\approx\boldsymbol{a}_0\cdot\boldsymbol{\nabla}_{\boldsymbol{\xi}_0}f^{(\mathrm{eq})}=-\frac{(\boldsymbol{\xi}_0-\boldsymbol{u}_0)\cdot\boldsymbol{a}_0}{RT}f^{(\mathrm{eq})}. \tag{31}$$

This formulation can ensure that the hydrodynamic equations at the Navier-Stokes order are the same as the original Boltzmann equation. It is noted that other consistent formulations, such as that proposed in Ref. [29], can also be used to approximate the forcing term. However, as can be seen in Sec. III, the use of Eq. (31) can make the final LBE model more concise. Based on Eq. (31), we can obtain easily the corresponding forcing terms in Eqs. (4) and (5) for the two reduced distribution functions,

$$\tilde{F}=\int Fd\xi_\theta=-\frac{(\boldsymbol{\xi}-\boldsymbol{u})\cdot\boldsymbol{a}}{RT}\tilde{f}^{(\mathrm{eq})},$$

$$\bar{F}=\int\xi_\theta Fd\xi_\theta=-\frac{(\boldsymbol{\xi}-\boldsymbol{u})\cdot\boldsymbol{a}}{RT}\bar{f}^{(\mathrm{eq})}-a_\theta\tilde{f}^{(\mathrm{eq})},$$

where $\boldsymbol{a}=(a_x,a_r)$. Therefore, the kinetic model with the body force can be expressed as

$$\frac{\partial\tilde{f}}{\partial t}+\boldsymbol{\xi}\cdot\boldsymbol{\nabla}\tilde{f}+\frac{\xi_r}{r}\tilde{f}=-\frac{1}{\tau}[\tilde{f}-\tilde{f}^{(\mathrm{eq})}]+\tilde{F}', \tag{32a}$$

$$\frac{\partial\bar{f}}{\partial t}+\boldsymbol{\xi}\cdot\boldsymbol{\nabla}\bar{f}+\frac{2\xi_r}{r}\bar{f}=-\frac{1}{\tau}[\bar{f}-\bar{f}^{(\mathrm{eq})}]+\bar{F}', \tag{32b}$$

where

$$\tilde{F}'=\frac{(\boldsymbol{\xi}-\boldsymbol{u})\cdot\tilde{\boldsymbol{a}}}{RT}\tilde{f}^{(\mathrm{eq})},\quad \bar{F}'=\frac{(\boldsymbol{\xi}-\boldsymbol{u})\cdot\bar{\boldsymbol{a}}}{RT}\bar{f}^{(\mathrm{eq})}+a_\theta\tilde{f}^{(\mathrm{eq})},$$

and

$$\tilde{a}_x=a_x,\quad \tilde{a}_r=a_r+\frac{RT}{r}\left(1+\frac{u_\theta^2}{RT}-\frac{2\tau u_r}{r}\right), \tag{33}$$

$$\bar{a}_x=a_x,\quad \bar{a}_r=a_r+\frac{RT}{r}\left(3+\frac{u_\theta^2}{RT}\right). \tag{34}$$

III. LATTICE BOLTZMANN MODEL FOR AXISYMMETRIC FLOWS

The two kinetic equations in Eq. (32) cannot be used to derive an efficient LBE model due to the last terms ($\xi_r\tilde{f}/r$ and $2\xi_r\bar{f}/r$) on the right-hand sides of them. In order to overcome the difficulties arising from these two terms, we rewrite Eq. (32) in more concise forms by multiplying them with r and r^2 on both sides, respectively,

$$\frac{\partial g}{\partial t} + \boldsymbol{\xi}\cdot\nabla g = -\frac{1}{\tau}[g - g^{(\mathrm{eq})}] + G, \tag{35a}$$

$$\frac{\partial h}{\partial t} + \boldsymbol{\xi}\cdot\nabla h = -\frac{1}{\tau}[h - h^{(\mathrm{eq})}] + H, \tag{35b}$$

where $g=r\tilde{f}$, $g^{(\mathrm{eq})}=r\tilde{f}^{(\mathrm{eq})}$, $G=r\tilde{F}'$, $h=r^2\bar{f}$, $h^{(\mathrm{eq})}=r^2\bar{f}^{(\mathrm{eq})}$, and $H=r^2\bar{F}'$. The fluid density and velocity are then computed as

$$\rho = \frac{1}{r}\int g\,d\boldsymbol{\xi}, \quad \rho\boldsymbol{u} = \frac{1}{r}\int \boldsymbol{\xi} g\,d\boldsymbol{\xi}, \quad \rho u_\theta = \frac{1}{r^2}\int h\,d\boldsymbol{\xi}. \tag{36}$$

Equations (35a) and (35b) are standard two-dimensional BGK models with a body force. Following the standard discretization procedure proposed in Refs. [30–33], we can obtain the following BGK models with nine discrete velocities:

$$\frac{\partial g_i}{\partial t} + \boldsymbol{c}_i\cdot\nabla g_i = -\frac{1}{\tau}[g_i - g_i^{(\mathrm{eq})}] + G_i, \tag{37a}$$

$$\frac{\partial h_i}{\partial t} + \boldsymbol{c}_i\cdot\nabla h_i = -\frac{1}{\tau}[h_i - h_i^{(\mathrm{eq})}] + H_i, \tag{37b}$$

where the discrete velocities $\{\boldsymbol{c}_i=(c_{ix},c_{ir}):i=0,1,\ldots,8\}$ are specified as $\boldsymbol{c}_0=0$, $\boldsymbol{c}_1=-\boldsymbol{c}_3=c(1,0)$, $\boldsymbol{c}_2=-\boldsymbol{c}_4=c(0,1)$, $\boldsymbol{c}_5=-\boldsymbol{c}_7=c(1,1)$, and $\boldsymbol{c}_6=-\boldsymbol{c}_8=c(-1,1)$, with $c=\sqrt{3RT}$. The discrete equilibrium distribution functions are obtained from the low Mach expansions of $g^{(\mathrm{eq})}$ and $h^{(\mathrm{eq})}$ [30,32],

$$g_i^{(\mathrm{eq})} = r\rho w_i\left[1 + \frac{\boldsymbol{c}_i\cdot\boldsymbol{u}}{c_s^2} + \frac{(\boldsymbol{c}_i\cdot\boldsymbol{u})^2}{2c_s^4} - \frac{|\boldsymbol{u}|^2}{2c_s^2}\right], \tag{38a}$$

$$h_i^{(\mathrm{eq})} = ru_\theta g_i^{(\mathrm{eq})}, \tag{38b}$$

where $c_s=\sqrt{RT}$ is the sound speed and the weights w_i are given by $w_0=4/9$, $w_{1\sim4}=1/9$, and $w_{5\sim8}=1/36$; the discrete forcing terms are given by

$$G_i = \frac{(\boldsymbol{c}_i-\boldsymbol{u})\cdot\tilde{\boldsymbol{a}}}{RT}g_i^{(\mathrm{eq})}, \quad H_i = \frac{(\boldsymbol{c}_i-\boldsymbol{u})\cdot\bar{\boldsymbol{a}}}{RT}h_i^{(\mathrm{eq})} + ra_\theta g_i^{(\mathrm{eq})}. \tag{39}$$

The fluid density and velocity are determined as follows:

$$\rho = \frac{1}{r}\sum_i g_i, \quad \rho\boldsymbol{u} = \frac{1}{r}\sum_i \boldsymbol{c}_i g_i, \quad \rho u_\theta = \frac{1}{r^2}\sum_i h_i. \tag{40}$$

Integrating Eq. (35) along the characteristic line from time t to $t+\delta_t$ leads to

$$g_i(\boldsymbol{x}+\boldsymbol{c}_i\delta_t,t+\delta_t) - g_i(\boldsymbol{x},t) = \int_0^{\delta_t}[\Omega_i^g(\boldsymbol{x}+\boldsymbol{c}_it',t+t') + G_i(\boldsymbol{x}+\boldsymbol{c}_it',t+t')]dt',$$

$$h_i(\boldsymbol{x}+\boldsymbol{c}_i\delta_t,t+\delta_t) - h_i(\boldsymbol{x},t) = \int_0^{\delta_t}[\Omega_i^h(\boldsymbol{x}+\boldsymbol{c}_it',t+t') + H_i(\boldsymbol{x}+\boldsymbol{c}_it',t+t')]dt',$$

where $\Omega_i^g=-[g_i-g_i^{(\mathrm{eq})}]/\tau$ and $\Omega_i^h=-[h_i-h_i^{(\mathrm{eq})}]/\tau$. As argued in [34], the integral on the right-hand side must be evaluated using a quadrature with at least second-order accuracy in order to obtain the correct hydrodynamic equations. The trapezoidal rule can serve this purpose and leads to the following implicit discrete schemes:

$$g_i(\boldsymbol{x}+\boldsymbol{c}_i\delta_t,t+\delta_t) - g_i(\boldsymbol{x},t) = \frac{\delta_t}{2}[\Omega_i^g(\boldsymbol{x},t) + G_i(\boldsymbol{x},t)] + \frac{\delta_t}{2}[\Omega_i^g(\boldsymbol{x}+\boldsymbol{c}_i\delta_t,t+\delta_t) + G_i(\boldsymbol{x}+\boldsymbol{c}_i\delta_t,t+\delta_t)], \tag{41}$$

$$h_i(\boldsymbol{x}+\boldsymbol{c}_i\delta_t,t+\delta_t) - h_i(\boldsymbol{x},t) = \frac{\delta_t}{2}[\Omega_i^h(\boldsymbol{x},t) + H_i(\boldsymbol{x},t)] + \frac{\delta_t}{2}[\Omega_i^h(\boldsymbol{x}+\boldsymbol{c}_i\delta_t,t+\delta_t) + H_i(\boldsymbol{x}+\boldsymbol{c}_i\delta_t,t+\delta_t)]. \tag{42}$$

The implicitness in the above schemes can be eliminated by introducing the following distribution functions as suggested in [34]:

$$\hat{g}_i = g_i - \frac{\delta_t}{2}(\Omega_i^g + G_i), \quad \hat{h}_i = h_i - \frac{\delta_t}{2}(\Omega_i^h + H_i). \tag{43}$$

Equations (41) and (42) can then be rewritten as explicit schemes,

$$\hat{g}_i(\boldsymbol{x}+\boldsymbol{c}_i\delta_t,t+\delta_t) - \hat{g}_i(\boldsymbol{x},t) = -\omega[\hat{g}_i(\boldsymbol{x},t) - g_i^{(\mathrm{eq})}(\boldsymbol{x},t)] + \delta_t\left(1-\frac{\omega}{2}\right)G_i(\boldsymbol{x},t), \tag{44}$$

$$\hat{h}_i(\boldsymbol{x}+\boldsymbol{c}_i\delta_t,t+\delta_t) - \hat{h}_i(\boldsymbol{x},t) = -\omega[\hat{h}_i(\boldsymbol{x},t) - h_i^{(\mathrm{eq})}(\boldsymbol{x},t)] + \delta_t\left(1-\frac{\omega}{2}\right)H_i(\boldsymbol{x},t), \tag{45}$$

where $\omega=2\delta_t/(2\tau+\delta_t)$. From Eqs. (43) and (40), it is can be easily shown that the fluid density and velocity can be determined from the new distribution functions as

$$\rho = \frac{1}{r}\sum_i \hat{g}_i, \quad \rho u_\theta = \frac{1}{r^2}\sum_i \hat{h}_i + \frac{\delta_t}{2}\rho a_\theta,$$

$$\rho u_\alpha = \frac{r}{r^2 + \tau\delta_t RT\delta_{\alpha r}}\left[\sum_i c_{i\alpha}\hat{g}_i + \frac{\delta_t}{2} r\rho a_\alpha + \frac{\delta_t}{2}\rho(RT + u_\theta^2)\delta_{\alpha r}\right]. \tag{46}$$

Equations (44) and (45) together with Eqs. (38) and (46) constitute our LBE model for axisymmetric flows when the physical space is discretized with a regular lattice with spacing $\delta_x = c\delta_t$.

Now some comments on the present model are in order. First, the present LBE model is derived from the kinetic model proposed in Sec. II which is based on the continuous Boltzmann equation and thus has a solid foundation. The advantage of this starting point also makes it easy to extend the present LBE model to other complicated fluid systems that can be described by kinetic models but may be difficult by macroscopical models. For instances, the model can be extended to nonideal fluids where intermolecular interactions are important and to microscale flows for which the Boltzmann equation is valid but the Navier-Stokes would fail. Second, in the present LBE model the velocities in the axial, radial, and azimuthal directions are all solved within the same LBE framework. This feature makes the implementation of the present LBE easier than the hybrid methods and is particularly useful for parallel computing. Third, unlike other existing axisymmetric LBE models, the forcing terms, G_i and H_i given by Eq. (39), are much simpler and contain no velocity gradients. Finally, the discrete lattice effects on the fluid velocity are considered in the present model, which is consistent with the analysis in Ref. [29].

We would also like to emphasize that the second equation of the proposed model [Eq. (45)] is for the azimuthal velocity, which has been neglected in most of previous axisymmetric LBE models. For flows with a negligible azimuthal velocity, Eq. (45) can be safely dropped, and the present LBE model contains only Eq. (44), which is similar to most of previous ones. On the other hand, if the azimuthal velocity must be considered, Eq. (45) should be invoked. In previous studies (e.g., Ref. [17]), some hybrid methods have been proposed where the macroscopic governing equation for the azimuthal velocity was solved using certain finite-difference schemes, which would lead to some additional computational effort comparable to that of Eq. (45). Furthermore, the different computation frameworks for the three velocity components in such hybrid methods may not only bring some difficulties in programming (particularly for parallel computations) but also may bring some inconsistency in accuracy because of the use of different computational stencils [35].

IV. BOUNDARY CONDITIONS AND FORCE EVALUATION

Specifying suitable boundary conditions for the distribution function(s) is an important topic in the study of LBE method in that it will not only influence the accuracy of the solution but also affect numerical stability of the algorithm significantly. Many different boundary conditions have been proposed for the standard LBE in the Cartesian coordinate, such as the simple bounce-back scheme [36], interpolation/extrapolation schemes [37–40], and hydrodynamic schemes

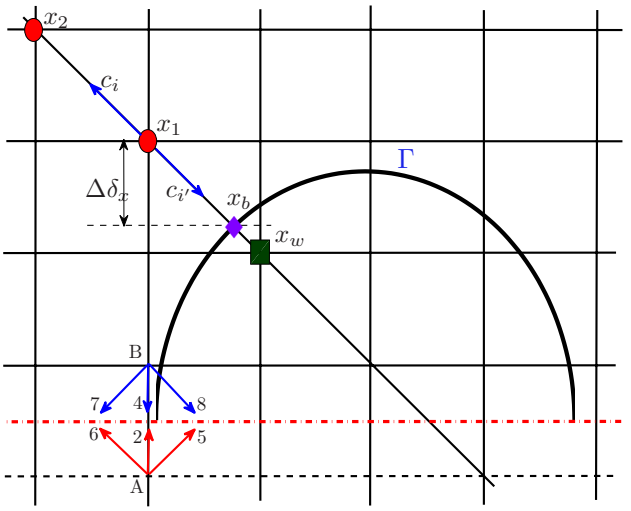

FIG. 1. (Color online) Nonequilibrium extrapolation method for a curved boundary. Solid square: ghost node in the body; solid circle: fluid node; solid diamond: intersection of the link along c_i with the boundary; dashed-dotted line: symmetry axis; and dashed line: ghost boundary along symmetry axis.

[41–43]. In this work we will extend the nonequilibrium extrapolation scheme (NEES) proposed in Ref. [38] to the present axisymmetric LBE model due to its simplicity, capability for different boundary conditions, second-order accuracy, and good numerical stability.

As depicted in Fig. 1, the distribution functions g_i and h_i at the fluid node x_1 near the boundary need to be determined by certain boundary conditions. In the NEES this is achieved by specifying the postcollision distribution functions $\hat{g}_i'$ and $\hat{h}_i'$ at the ghost node x_w located in the wall, where

$$\hat{\varphi}_i' = \hat{\varphi}_i - \omega[\hat{\varphi}_i - \varphi_i^{(\mathrm{eq})}] + \delta_t\left(1 - \frac{\omega}{2}\right)S_i, \tag{47}$$

with $\varphi_i = g_i$ or h_i and $S_i = G_i$ or H_i. Once $\hat{\varphi}_i'$ is known, $\hat{\varphi}_i(\boldsymbol{x}_1, t+\delta_t)$ can be obtained by performing a simple streaming operation, i.e., $\hat{\varphi}_i(\boldsymbol{x}_1, t+\delta_t) = \hat{\varphi}_i'(\boldsymbol{x}_w, t)$. The basic ideas of NEES are to decompose the distribution function at $\boldsymbol{x}_w$ into its equilibrium and nonequilibrium parts, $\hat{\varphi}_i = \varphi_i^{(\mathrm{eq})} + \hat{\varphi}_i^{(\mathrm{neq})}$, and then approximate the first part with a ghost equilibrium with extrapolated velocity and density, while the second part is approximated with extrapolations directly [38]. NEES has been proved to be of second-order accuracy and have good numerical stability for LBE models in the Cartesian coordinate. With the same idea, the NEES can be generalized for the present axisymmetric LBE model, in which the postcollision distribution function at $\boldsymbol{x}_w$ is constructed as

$$\hat{\varphi}_i'(\boldsymbol{x}_w) = E_{\varphi i}(\rho_w, \boldsymbol{u}_w) + (1-\omega)\hat{\varphi}_i^{(\mathrm{neq})}(\boldsymbol{x}_w) + \frac{2-\omega}{2}S_i\delta_t, \tag{48}$$

where $E_{\varphi i} = \varphi_i^{(\mathrm{eq})}$, $\rho_w = \rho(\boldsymbol{x}_1, t)$, and

$$\boldsymbol{u}_w = \begin{cases} \dfrac{(3-\Delta)\boldsymbol{u}(\boldsymbol{x}_b) + (\Delta^2-1)\boldsymbol{u}(\boldsymbol{x}_1) - (1-\Delta)^2\boldsymbol{u}(\boldsymbol{x}_2)}{1+\Delta}, & \Delta < 0.75, \\ \dfrac{\boldsymbol{u}(\boldsymbol{x}_b) + (\Delta-1)\boldsymbol{u}(\boldsymbol{x}_1)}{\Delta}, & \Delta \geq 0.75, \end{cases} \tag{49}$$

$$\hat{\varphi}_i^{(\mathrm{neq})}(\boldsymbol{x}_w) = \begin{cases} \Delta\hat{\varphi}_i^{(\mathrm{neq})}(\boldsymbol{x}_1) + (1-\Delta)\hat{\varphi}_i^{(\mathrm{neq})}(\boldsymbol{x}_2), & \Delta < 0.75, \\ \hat{\varphi}_i^{(\mathrm{neq})}(\boldsymbol{x}_1), & \Delta \geq 0.75. \end{cases} \tag{50}$$

Here, $\Delta = |\boldsymbol{x}_1 - \boldsymbol{x}_b| / |\boldsymbol{x}_1 - \boldsymbol{x}_w|$ is the fraction of the intersected link in the fluid region along $\mathbf{c}_i$, and the nonequilibrium distribution function of $\hat{\varphi}_i$ at $\boldsymbol{x}_1$ or $\boldsymbol{x}_2$ is given by $\hat{\varphi}_i^{(\mathrm{neq})} = \hat{\varphi}_i - \varphi_i^{(\mathrm{eq})}$.

Boundary conditions at a wall reflect the interactions between fluid and the boundary. Momentum exchange between the fluid and the wall will occur during the interaction process. After collision at time t, the quantity $\boldsymbol{c}_{i'}\hat{g}_{i'}(\boldsymbol{x}_1)/r_1$ represents the total momentum of the particles moving with $\boldsymbol{c}_{i'} = -\boldsymbol{c}_i$ in the $\boldsymbol{x} = (x, r)$ plane at x_1. During one time step, these particles interact with the wall at $\boldsymbol{x}_b$ and the momentum they carry becomes $\boldsymbol{c}_i\hat{g}_i(\boldsymbol{x}_1, t+\delta_t)/r_1$. This means that these particles exert a force on the wall at point $\boldsymbol{x}_b$,

$$\begin{aligned} \boldsymbol{F}(x_b, t) &= -\frac{\boldsymbol{c}_i\hat{g}_i(x_1, t+\delta_t) - \boldsymbol{c}_{i'}\hat{g}_{i'}(\boldsymbol{x}_1, t)}{r_1\delta_t} \\ &= -\frac{\boldsymbol{c}_i}{\delta_t}\left[\frac{\hat{g}_i'(x_w, t)}{r_w} + \frac{\hat{g}_{i'}(\boldsymbol{x}_1, t)}{r_1}\right]. \end{aligned} \tag{51}$$

For an axisymmetric body where the axis lies along the x direction, the total drag force exerted by the fluid is therefore

$$\begin{aligned} F_x &= 2\pi\int_\Gamma \delta_x r F_x(\boldsymbol{x}) dl \approx 2\pi\sum_{\boldsymbol{x}_b\in\Gamma} r_b F_x(\boldsymbol{x}_b)\delta_x^2 \\ &\approx -\frac{\delta_x^2}{\delta_t}[\hat{g}_i'(x_w, t) + \hat{g}_{i'}(\boldsymbol{x}_1, t)]2\pi\boldsymbol{c}_{ix}, \end{aligned} \tag{52}$$

where Γ is the body surface in the meridian half-plane.

Another important boundary condition for axisymmetric flow is the treatment of the axis of symmetry. In order to avoid the singularity at $r=0$, we set the first lattice line at $r = 0.5\delta_x$ and apply the following symmetry boundary condition to a ghost lattice line located at $r = -0.5\delta_x$ (see Fig. 1):

$$\hat{\varphi}_2'(A) = \hat{\varphi}_4'(B), \quad \hat{\varphi}_5'(A) = \hat{\varphi}_8'(B), \quad \hat{\varphi}_6'(A) = \hat{\varphi}_7'(B), \tag{53}$$

where A is the symmetric ghost node of B located at the first fluid line.

V. NUMERICAL RESULTS

In this section we shall validate the proposed LBE model by some well-studied axisymmetric flows, including steady and unsteady tube flows, the flows around a sphere, and the swirling flows in a cylindrical cavity. In our simulations, the symmetry boundary condition described in Sec. IV will be used for the symmetry axis in each case, and the NEES will be employed to treat different boundary conditions for other boundaries.

A. Flow in a pipe

The first test case is the Hagen-Poiseuille flow through a straight pipe of radius $R=1.0$ driven by a constant external force $\boldsymbol{a} = (a_x, 0, 0)$. The computational domain is $0 \leq x \leq 0.1$ and $0 \leq r \leq R$, where $r=0$ is the symmetric axis and the solid wall is located at $r=R$. The boundary conditions for the fluid variables are as follows:

$$r = 0: \quad \frac{\partial\varphi}{\partial r} = 0, \quad \forall\ \varphi;$$

$$r = R: \quad u_x = u_r = u_\theta = 0.$$

In the streamwise direction, periodic boundary conditions are applied to both the entrance and outlet. With these conditions, the steady axial velocity reads

$$u_x(r) = u_0\left(1 - \frac{r^2}{R^2}\right), \tag{54}$$

where $u_0 = a_x R^2/4\nu$ is the maximum velocity. The radial and azimuthal velocities are both zero for this problem.

Since the azimuthal component of the velocity is vanishing, we can use Eq. (44) solely in simulations. However, in order to test the performance of the proposed LBE model as a whole, here we still apply the complete version of the model [Eqs. (44) and (45)] to the Hagen-Poiseuille with different lattice sizes and relaxation times. Periodic boundary conditions are applied to the entrance and exit, and the NEES is applied to the solid wall. Figure 2 compares the velocity predicted by the present LBE with the analytical solutions for $\mathrm{Re} = 2Ru_0/\nu = 40$. The results are obtained based on a lattice with resolution $\delta_x = R/16$, and two values of the relaxation time, $\tau = 0.75$ and 1.25, are used. It is seen that the numerical results agree excellently with the analytical one. In Fig. 3 the relative global errors in velocity with different mesh resolutions are presented. Here the relative global error is defined as

$$E(u) = \frac{\|u_c - u_x\|_2}{\|u_x\|_2}, \tag{55}$$

where u_c is axial velocity predicted by the LBE and u_x is the analytical solution. The slops of the fittings to the errors in the cases of $\tau = 1.25$ and 0.75 are 2.006 and 1.973, respec-

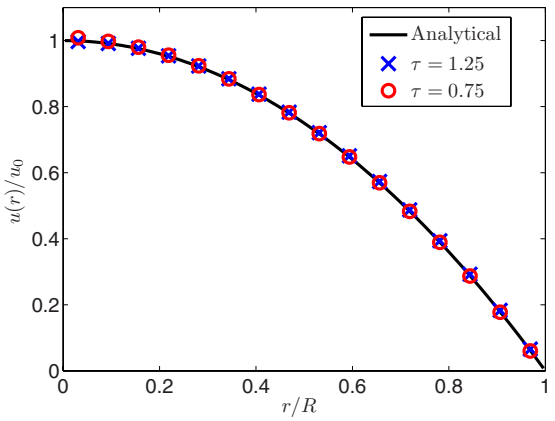

FIG. 2. (Color online) Velocity of the Poiseuille flow (Re=40, $\delta_x = R/16$).

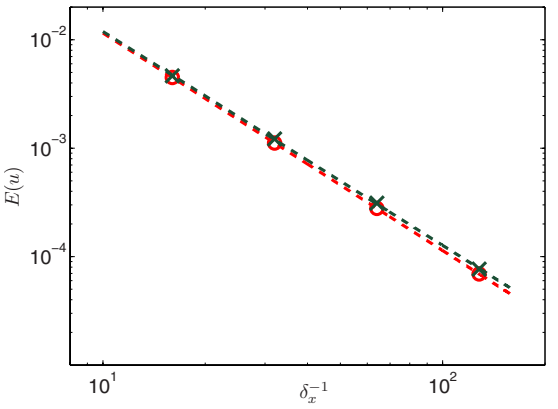

FIG. 3. (Color online) Relative global errors against lattice spacing δ_x at Re=40. ○: τ=1.25; ×: τ=0.75. Dashed lines are the two least-squares fittings and the slopes are 2.006 and 1.973, respectively.

tively, which show that the LBE is of second-order accuracy in space. The radial and azimuthal velocities are also measured. It is found that u_θ is exactly zero everywhere, while u_r/u_0 is in the order of 10^{-17}.

In the Hagen-Poiseuille flow the driven force is a constant. If the force oscillates with a period $T=2\pi/\Omega$, i.e., $a_x = G\cos(\Omega t)$, the flow will become the pulsatile Womersley flow and admits an analytical solution

$$u_x(r,t) = \mathrm{Re}\left\{\frac{G}{i\Omega}\left[1 - \frac{J_0(rs/R)}{J_0(s)}\right]e^{i\Omega t}\right\}, \qquad (56)$$

where $s=\alpha(i-1)/\sqrt{2}$, $\alpha=R\sqrt{\Omega/\nu}$ is the Womersley number, i is the imaginary unit, and J_0 is the zeroth-order Bessel function of the first type, and "Re" means the real part of a complex variable.

In simulations the boundary conditions are the same as used in the Poiseuille flow. Initially the velocity is set to be zero everywhere, and numerical results are measured after running ten periods. A set of simulations for different Womersley number and Reynolds number is performed. Here the Reynolds number is defined as $\mathrm{Re}=2Ru_0/\nu$ with $u_0 = GR^2/4\nu$. In Fig. 4 the numerical solutions as well as the analytical ones are shown at four different times for $\alpha=8$ and 16 at Re=1200. It can be seen that the numerical solutions are in excellent agreement with the analytical ones. The mesh resolution is set to be $\delta_x = R/20$ for $\alpha=8$, and the relaxation time is taken to be 0.6. With these parameters, $G \approx 6.667\times10^{-3}$ and $T\approx1178$. As α increases to 16, the resolution is insufficient and we choose $\delta_x = R/80$. Correspondingly, in this case $G\approx4.167\times10^{-4}$ and $T\approx4712$. These parameters can ensure that the Mach number of the flow is sufficiently small so that the LBE is consistent with the incompressible Navier-Stokes equations.

B. Flow over a sphere

The external flow over a sphere has been well studied both experimentally and numerically [44–50] and can serve as a good benchmark problem for numerical schemes. Previous studies show that as the Reynolds number (Re) is less than 200, the flow developed a steady axisymmetric wake. Here Re is based on the free-stream velocity u_0 and the diameter of the sphere. In this work we will simulate this flow as Re ranges from 5 to 120, The simulation domain is 0

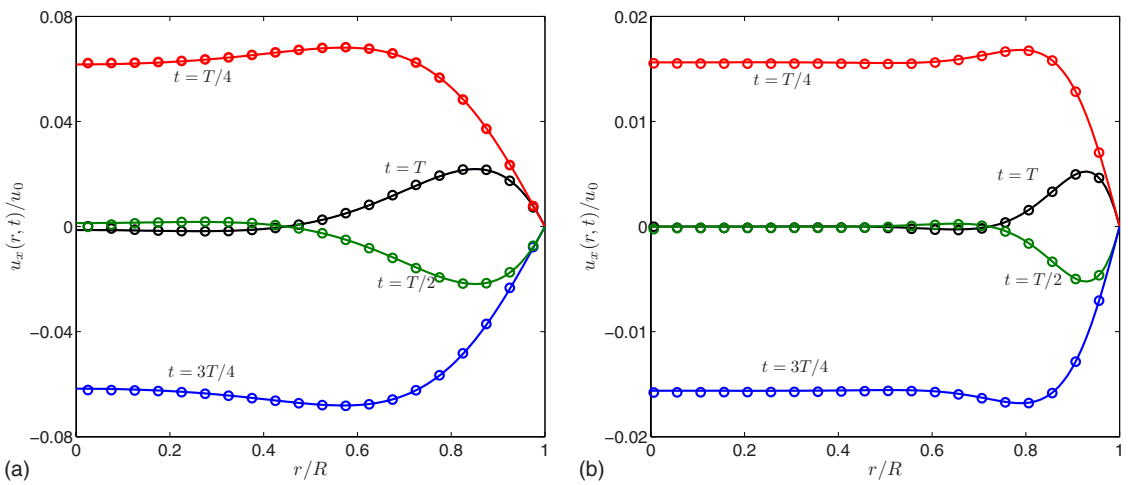

FIG. 4. (Color online) Velocity of the Womersley flow (Re=1200, τ=0.6). (a) α=8, $\delta_x = R/20$; (b) α=16, $\delta_x = R/80$.

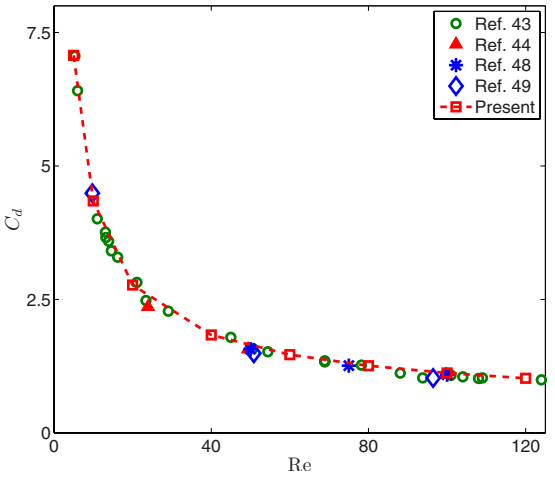

FIG. 5. (Color online) Drag coefficient against the Reynolds number ($\delta_x = R/16$).

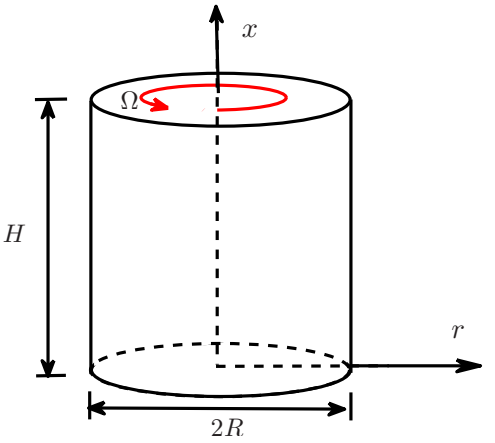

FIG. 6. (Color online) Schematic of the cylindrical cavity flow.

$\leq x \leq 40R$ and $0 \leq r \leq 10R$, where $R=0.05$ is the radius of the sphere, and the center of the sphere is placed at $(20R, 0)$.

No slip boundary condition is assumed at the surface of the sphere, and the free-stream boundary conditions $u_x = u_0$, $u_r = u_\theta = 0$ are applied at the inflow boundary. The convection boundary conditions, $\partial_t \varphi + u_0 \partial_x \varphi = 0$ ($\varphi = \rho, u_x, u_r, u_\theta$), are applied to the outflow boundary; at the side boundary, we set $\partial_r \varphi = 0$.

The flow can be assumed to be nonswirling as done in many of previous studies. As such, in our simulations we will drop Eq. (45) from the LBE model and use Eq. (44) for

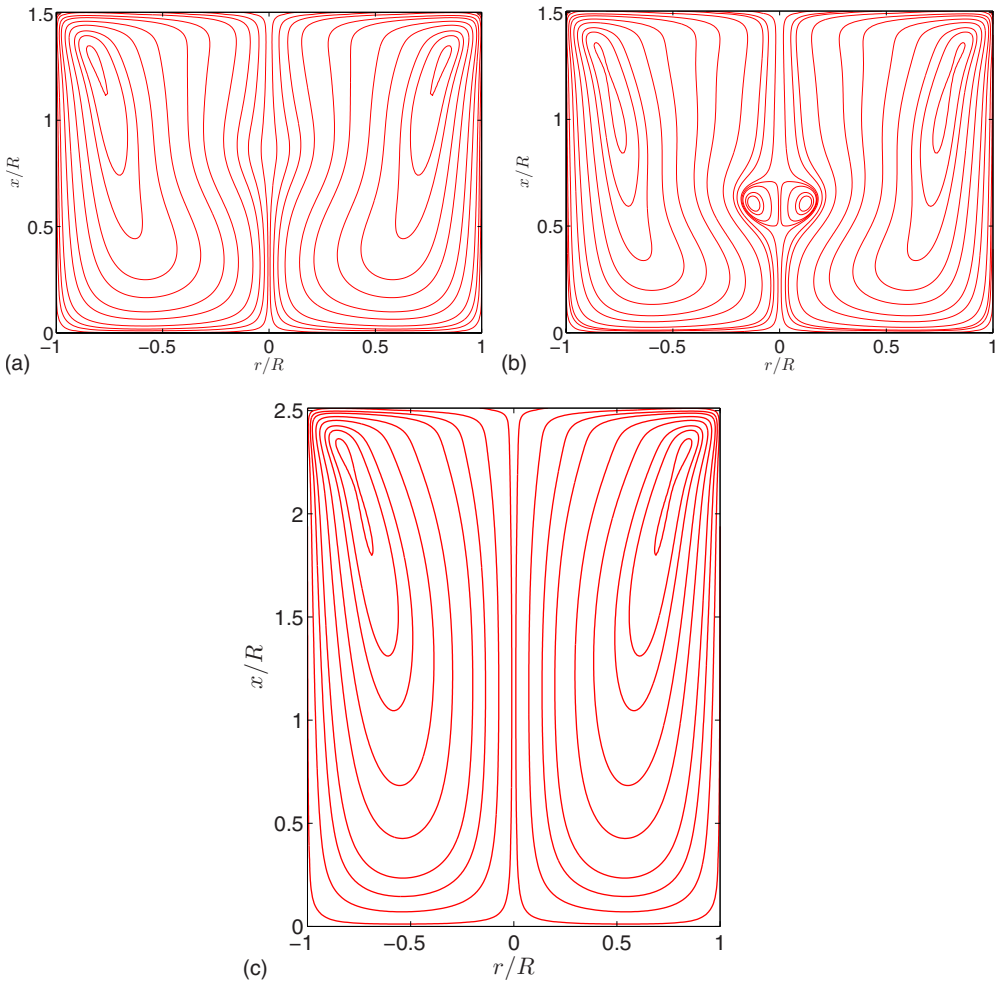

FIG. 7. (Color online) Streamline of the cylindrical cavity flow in the meridianal plane. (a) Case A ($R_A = 1.5$, Re=990), (b) case B ($R_A = 1.5$, Re=1290), and (c) case C ($R_A = 2.5$, Re=1010).

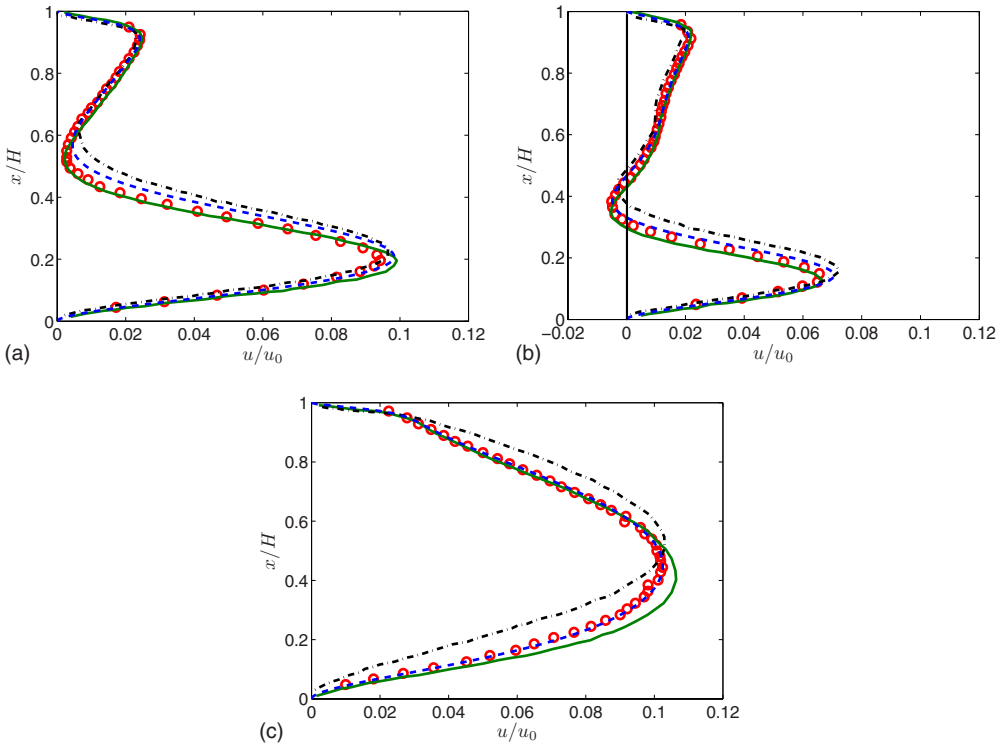

FIG. 8. (Color online) Axial velocity on the axis ($u_0=\Omega R$). (a) Case A ($R_A=1.5$, Re=990), (b) case B ($R_A=1.5$, Re=1290), and (c) case C ($R_A=2.5$, Re=1010). Circle: experimental [56], solid line: Navier-Stokes [57], dashed-dotted line: 3D LBE [57], and dashed line: present LBE.

the axial and radial velocities. The boundary conditions in terms of macroscopical variables mentioned above are implemented in the proposed LBE through the NEES as follows. The inflow free-stream velocity boundary conditions and the no slip boundary condition at the sphere are treated directly by the NEES as described in Sec. IV; at the outflow boundary, we first obtain the velocity and density at the boundary by solving the differential equation using an implicit first-order upwind finite-difference scheme and then transfer them to the distribution function $\hat{g}_i$ via the NEES. The side boundary is treated similarly.

A mesh with size $N_x \times N_r = 641 \times 162$ is used in the simulations. The resolution is enough for the Reynolds numbers considered here. The free-stream velocity u_0 is set to be 0.1, and the relaxation time is given by $\tau = 2Ru_0/\mathrm{Re}c_s^2\delta_t$. At each Re, a steady state is reached after a number of iterations, where the steady criterion is

$$\frac{\|\boldsymbol{u}(t) - \boldsymbol{u}(t - 1000\delta_t)\|}{\|\boldsymbol{u}(t)\|} < 10^{-6},$$

namely, it is based on the relative error of the velocity field between two successive 1000 time steps. Here the norm is defined as $\|\boldsymbol{u}\| = [\Sigma_{x,r} u_x^2(x,r) + u_r^2(x,r)]^{1/2}$, where the summation is taken over the whole computation domain.

At the steady state, the drag force exerted on the sphere is measured according to Eq. (52). In Fig. 5 the drag coefficients, $C_d = 4F_x/\rho u_0^2 R^2$, are shown and compared with published data in previous studies for $5 \le \mathrm{Re} \le 120$. Clearly the LBE results are in quantitative agreement with existing experimental and numerical data.

C. Cylindrical cavity flow

The azimuthal velocity vanishes in both the tube flow and the flow over a sphere. In this section we will validate the proposed LBE model by the swirling flow in a closed cylindrical cavity where u_θ plays a dominant role. The schematic of the problem is shown in Fig. 6. The radius of the cavity is R and the height is H. The bottom of the cavity is closed and kept stationary, while the top lid rotates around the cylindrical axis with a constant angular velocity Ω.

Previous studies (e.g., [51–56]) have shown that the flow structure depends on two key dimensionless parameters, i.e., the aspect ratio $R_A = H/R$ and the rotational Reynolds number $\mathrm{Re} = \Omega R^2/\nu$. With different combinations of these two parameters, distinct breakdown bubbles may occur. Owing to the simple geometry and the ease in establishing boundary conditions, the cylindrical cavity flow has been the subject of a large number of numerical studies based on the Navier-Stokes equations. A recent fully three-dimensional lattice Boltzmann simulation was also carried out to determine the interior flow structure [57].

We shall validate the present axisymmetric LBE model by the cylindrical cavity flow with three sets of (R_A,Re), namely (A) (1.5, 990), (B) (1.5, 1290), and (C) (2.5,1010), which correspond to the cases in the experimental study [56] and lattice Boltzmann simulation [57]. The computations are based on a lattice with $\delta_x = R/100$. The boundary conditions

are set as follows: $u_x=u_r=u_\theta=0$ for the bottom and outer walls and $u_x=u_r=0$ and $u_\theta=\Omega r$ for the top rotating wall. The NEES is employed to realize these velocity boundary conditions, and the symmetry boundary condition is applied to the axis.

In Fig. 7 the streamlines of the swirling flow are shown for the three cases considered. It is seen that in the cases of (A) and (C), no breakdown bubbles are seen; in case (B), however, a single bubble appears. The flow structures in these cases are consistent with previous experimental and numerical results [56,57]. To quantify the comparison, the axial velocity u_x on the axis predicted by the present LBE is shown in Fig. 8 where the experimental data [56], the Navier-Stokes solutions [57], and the three-dimensional (3D) LBE results are also presented. Here u_x on the axis is obtained by extrapolating the values on the two nearest neighboring nodes, i.e., $u(x,0)=[9u_x(x,0.5\delta_x)-u_x(x,1.5\delta_x)]/8$, where we have made use of the symmetric property of u_x. Clearly the present LBE results are in good agreement with the experimental and numerical ones. It is also noticeable that the present results just lie between the Navier-Stokes and the full 3D LBE solutions.

VI. SUMMARY

In this work a LBE model for axisymmetric flows is developed starting from the continuous Boltzmann-BGK equation. By introducing two reduced distributions, a simplified kinetic model is first proposed which can lead to the same hydrodynamic equations as the original one. Then, after some standard discretizations and a variable transformation, an explicit LBE model is obtained. Compared with existing axisymmetric LBE models, the present one has the following advantages: (i) it is based on the kinetic equation and thus has a solid foundation and can be extended to other fluid systems following similar approaches; (ii) it can solve the axial, radial, and azimuthal velocity within the same framework and is more easy for practical applications; (iii) it has a much simpler structure and contains no velocity gradients that exist in most of other axisymmetric LBE models. These advantages enable the present model an ideal tool for simulating axisymmetric flows.

A set of numerical simulations are carried out to test the performance of the proposed LBE model. The test problems include steady/unsteady tube flows, external flow around a sphere, and internal swirling flow in a cylindrical cavity. Numerical results are compared with analytical, numerical, and/or experimental results in previous studies, and the comparisons show the reliability of the present model.

In the present work the LBE model utilizes a BGK operator with a unique single relaxation time; more advanced collision model with multiple relaxation times (MRT) [35,58] can also be employed and a MRT model is expected to have better numerical stability. The nonequilibrium extrapolation boundary condition is employed here, but this does not prevent the model from using other boundary conditions. It is also interesting to make some performance comparisons between LBE models with different approximations to $\tilde{\phi}$ and $\bar{\phi}$. We will study these issues in our future work.

ACKNOWLEDGMENTS

This work was supported by the National Natural Science Foundation of China (Grants No. 50606012 and No. 50721005) and the Program for NCET in university (Grant No. NCET-07-0323).

[1] R. Benzi, S. Succi, and M. Vergassola, Phys. Rep. **222**, 145 (1992).
[2] Y. H. Qian, S. Succi, and S. A. Orszag, in *Recent Advances in Lattice Boltzmann Computing*, Annual Reviews of Computational Physics Vol. III, edited by Dietrich Stauffer (World Scientific, Singapore, 1996), pp. 195–242.
[3] S. Chen and G. D. Doolen, Annu. Rev. Fluid Mech. **30**, 329 (1998).
[4] L.-S. Luo, in Proceedings of the International Conference on Applied Computational Fluid Dynamics, Beijing, China, 2000, edited by J.-H. Wu and Z.-J. Zhu, pp. 52–83. Available at http://www.lions.odu.edu/~lluo/nonjournal-pubs.html.
[5] S. Succi, *The Lattice Boltzmann Equation for Fluid Dynamics and Beyond* (Oxford University Press, Oxford, 2001).
[6] R. S. Maier, R. S. Bernard, and D. W. Grunau, Phys. Fluids **8**, 1788 (1996).
[7] A. M. Artoli, A. G. Hoekstra, and P. M. A. Sloot, Int. J. Mod. Phys. C **13**, 1119 (2002).
[8] S. K. Bhaumik and K. N. Lakshmisha, Comput. Fluids **36**, 1163 (2007).
[9] I. Halliday, L. A. Hammond, C. M. Care, K. Good, and A. Stevens, Phys. Rev. E **64**, 011208 (2001).
[10] K. N. Premnath and J. Abraham, Phys. Rev. E **71**, 056706 (2005).
[11] S. Mukherjee and J. Abraham, Phys. Rev. E **75**, 026701 (2007).
[12] T. S. Lee, H. Huang, and C. Shu, Int. J. Mod. Phys. C **17**, 645 (2006).
[13] T. Reis and T. N. Phillips, Phys. Rev. E **75**, 056703 (2007).
[14] T. Reis and T. N. Phillips, Phys. Rev. E **77**, 026703 (2008).
[15] J. G. Zhou, Phys. Rev. E **78**, 036701 (2008).
[16] S. Chen, J. Tölke, S. Geller, and M. Krafczyk, Phys. Rev. E **78**, 046703 (2008).
[17] Y. Peng, C. Shu, Y. T. Chew, and J. Qiu, J. Comput. Phys. **186**, 295 (2003).
[18] X. D. Niu, C. Shu, and Y. T. Chew, Int. J. Mod. Phys. C **14**, 785 (2003).
[19] M. E. McCracken and J. Abraham, Int. J. Mod. Phys. C **16**, 1671 (2005).
[20] D. Hänel, U. Lantermann, and R. Kaiser, in *Proceedings of the 3rd International Conference on Computational Fluid Dynamics, Toronto, 2004*, edited by C. Groth and D. W. Zingg

(Springer-Verlag, Berlin, 2006), pp. 587–592.
[21] H. Huang, T. S. Lee, and C. Shu, Int. J. Numer. Methods Fluids **53**, 1707 (2007).
[22] H. Huang, T. S. Lee, and C. Shu, Int. J. Numer. Methods Heat Fluid Flow **17**, 587 (2007).
[23] T. S. Lee, H. Huang, and C. Shu, Int. J. Numer. Methods Fluids **49**, 99 (2005).
[24] S. Mukherjee and J. Abraham, J. Colloid Interface Sci. **312**, 341 (2007).
[25] S. Mukherjee and J. Abraham, Phys. Fluids **19**, 052103 (2007).
[26] L. Mieussens, J. Comput. Phys. **162**, 429 (2000).
[27] T. Inamuro, A. Yamaguchi, and F. Ogino, Fluid Dyn. Res. **21**, 417 (1997).
[28] X. He, X. Shan, and G. D. Doolen, Phys. Rev. E **57**, R13 (1998).
[29] Z. Guo, C. Zheng, and B. Shi, Phys. Rev. E **65**, 046308 (2002).
[30] X. He and L.-S. Luo, Phys. Rev. E **55**, R6333 (1997).
[31] X. He and L.-S. Luo, Phys. Rev. E **56**, 6811 (1997).
[32] X. Shan and X. He, Phys. Rev. Lett. **80**, 65 (1998).
[33] X. Shan, X.-F. Yuan, and H. Chen, J. Fluid Mech. **550**, 413 (2006).
[34] X. He, S. Chen, and G. D. Doolen, J. Comput. Phys. **146**, 282 (1998).
[35] P. Lallemand and L.-S. Luo, Phys. Rev. E **68**, 036706 (2003).
[36] X. He, Q. Zou, L.-S. Luo, and M. Dembo, J. Stat. Phys. **87**, 115 (1997).
[37] S. Chen, D. Martinez, and R. Mei, Phys. Fluids **8**, 2527 (1996).
[38] Z. L. Guo, C. G. Zheng, and B. C. Shi, Phys. Fluids **14**, 2007 (2002).
[39] M. Bouzidi, M. Firdaouss, and P. Lallemand, Phys. Fluids **13**, 3452 (2001).
[40] I. Ginzburg and D. d'Humiéres, Phys. Rev. E **68**, 066614 (2003).
[41] D. R. Noble, S. Chen, J. G. Georgiadis, and R. O. Buckius, Phys. Fluids **7**, 203 (1995).
[42] T. Inamuro, M. Yoshino, and F. Ogino, Phys. Fluids **7**, 2928 (1995).
[43] Q. Zou and X. He, Phys. Fluids **9**, 1591 (1997).
[44] F. W. Roos and W. W. Willmarth, AIAA J. **9**, 285 (1971).
[45] T. A. Johnson and V. C. Patel, J. Fluid Mech. **378**, 19 (1999).
[46] A. Gilmanov, F. Sotiropoulos, and E. Balaras, J. Comput. Phys. **191**, 660 (2003).
[47] X. Y. Wang, K. S. Yeo, C. S. Chew, and B. C. Khoo, Comput. Fluids **37**, 733 (2008).
[48] R. Clift, R. J. Grace, and E. W. Weber, *Bubbles, Drops, and Particles* (Academic, New York, 1978).
[49] R. Mittal, Int. J. Numer. Methods Fluids **30**, 921 (1999).
[50] Y. Rimon and S. I. Cheng, Phys. Fluids **12**, 949 (1969).
[51] M. P. Escudier, Exp. Fluids **2**, 189 (1984).
[52] H. J. Lugt and H. J. Haussling, ASME Trans. J. Appl. Mech. **49**, 921 (1982).
[53] H. J. Lugt and M. Abboud, J. Fluid Mech. **179**, 179 (1987).
[54] J. M. Lopez, J. Fluid Mech. **221**, 533 (1990).
[55] G. L. Brown and J. M. Lopez, J. Fluid Mech. **221**, 553 (1990).
[56] K. Fujimura, H. S. Koyama, and J. M. Hyun, ASME Trans. J. Fluids Eng. **119**, 450 (1997).
[57] S. K. Bhaumik and K. N. Lakshmisha, Comput. Fluids **36**, 1163 (2007).
[58] P. Lallemand and L.-S. Luo, Phys. Rev. E **61**, 6546 (2000).